Quantum Electronics **48** (11) 1009–1015 (2018)

QUANTUM TECHNOLOGY

https://doi.org/10.1070/QEL16699

Charge qubit under optical control in a thin semiconductor slab

A.V. Tsukanov, I.Yu. Kateev

Abstract. **The dynamics of a single-electron double quantum dot (charge qubit) in an optical microcavity has been theoretically analysed taking into account the influence of optical and acoustic phonons. The Lamb modes of a two-dimensional mechanical resonator (thin slab) are considered as an example of an acoustic phonon subsystem. It is found that an optical phonon mode can be used as a qubit control tool, similar to the microcavity photon one. The probability of the quantum operation 'NOT' has been calculated for two qubit control scenarios: in the microcavity photon field and in the combined photon–phonon field of a microcavity and slab. It is shown that the coherent energy exchange between a qubit and a set of acoustic phonon modes reduces this probability, which depends on the number of modes, the initial state of the phonon field, and the decay rate of modes.**

Keywords: *quantum computer, qubit, quantum dot, microcavity, acoustic phonons.*

1. Introduction

A semiconductor double quantum dot (DQD), consisting of two tunnel-coupled quantum dots (QDs) and containing one excess electron in the quantised part of the conduction band of a confining potential, can be considered as a two-level system (qubit) [1–5]. The two logical states of a charge DQD qubit are associated with localised single-electron orbitals in each QD. An arbitrary state of a qubit is set by their linear superposition. The possibility of controlling this qubit was experimentally demonstrated for a DQD based on two-dimensional electron gas in a GaAs/AlGaAs heterostructure [5]. An important feature of this system is that the qubit parameters change with variation in the electric potential on the control gates [5, 6] and/or the frequency and amplitude of the optical (laser [7] or microcavity [8]) field.

However, there are processes destroying the qubit state coherence, which are related to the solid-state environment of the DQD. An electron located in a DQD interacts with the mechanical stress field, described by longitudinal (LO) and transverse (TO) optical lattice vibrations (phonons) and longitudinal (LA) and transverse (TA) acoustic phonons [9]. Recall that the main relaxation channel for an excited electron in three-dimensional (crystals) or two-dimensional (quantum wells) semiconductors is emission of an LO phonon, which is caused by the Frohlich interaction and occurs for a time on the order of 1 ps. In point systems (QDs), due to the discreteness of the energy spectrum and weak dispersion of LO phonons, a qualitative analysis (based on the energy conservation law) predicts a rather low rate for LO phonon scattering. This statement is valid if the frequency ω_a of the electron transition in the QD (the energy difference between the ground and first excited electron states) differs from the LO phonon frequency (hereinafter, frequencies are given in energy units), which lies, e.g., for GaAs, in a narrow range, centred at 36.2 meV (the phonon bottleneck effect [10]). In this case, the relaxation of the excited electron is due to the hybridisation of the electron and phonon degrees of freedom and formation of a polaron, whose anharmonic decay is accompanied by emission of several acoustic phonons [11]. In crystalline QDs grown by the Stranski–Krastanov method, the transition frequency ranges from several tens of meV to 0.1 eV. The decay rate may depend nontrivially on the transition frequency and vary by several orders of magnitude within a given frequency range [12]. Therefore, choosing properly the ω_a value, one can slow down significantly the polaron anharmonic relaxation. Another dissipative channel is related to LA phonons, which are described in the deformation potential approximation. Their interaction with DQDs is weak in comparison with the Frohlich effects in three-dimensional crystals [13]. The energy of LA phonons at which their density in crystal is significant (from zero to several meV) is much lower than the transition energy between the DQD ground and excited states, while the probability of the corresponding scattering event is small, because the transition energy in such QDs exceeds 1 meV [14].

This conclusion is valid if the QD spectrum is described well within the two-level approximation. However, the presence of several closely spaced (or even degenerate) excited states of different symmetry leads to combined relaxation, including the transition between these states with emission/absorption of an acoustic phonon [12]. In addition, the DQDs whose spectrum contains hybridised excited orbitals may be involved in processes with participation of phonons whose energy corresponds to the level-splitting energy. The purpose of this study was to analyse the influence of a set of quasi-discrete acoustic modes on the qubit evolution. Under the assumption that DQDs and modes can exchange energy coherently, we calculate the time dependences of the electron transfer probability between ground states. Using a set of acoustic modes as a reservoir model, we obtain dependences of the maximum transfer probability on the interaction energy of these modes with the DQD electron and their decay rates.

A.V. Tsukanov, I.Yu. Kateev Valiev Institute of Physics and Technology, Russian Academy of Sciences, Nakhimovskii prosp. 34, 117218 Moscow, Russia; e-mail: ikateyev@mail.ru

Received 11 April 2018; revision received 16 July 2018
Kvantovaya Elektronika **48** (11) 1009–1015 (2018)
Translated by Yu.P. Sin'kov

As will be shown below, this probability depends also on the initial state of phonon field (coherent or thermal).

2. Model and basic equations

In this study, the quantum single-photon field of a single-mode microcavity with a mode frequency ω_c is used as an optical field inducing the desired quantum evolution of the charge DQD qubit (Fig. 1). An LO mode with a frequency ω_{LO} can also be applied to excite an optical transition in DQDs [15]. We model the dynamics of the hybrid DQD–microcavity–phonons system, assuming reversible energy exchange between the subsystems. This situation may occur in low-dimensional semiconductor structures (slabs, rods) whose phonon spectrum is characterised by a high degree of discreteness [16]. If the phonon mode frequencies lie in the vicinity of the DQD transition and microcavity frequency, an electron excitation in the DQD may be coherently transformed into a microcavity photon or phonons of the structure. In this case, complex oscillations of basis-state populations are observed in the hybrid system. An analogue of our system is a microwave-controlled superconducting phase qubit, which can exchange quantum energy with an electromechanical nanocavity based on aluminium nitride [17].

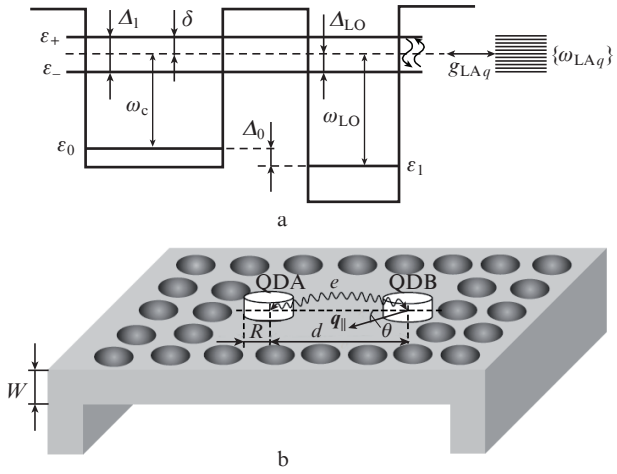

Figure 1. (a) Potential profile of a DQD qubit and (b) schematic image of a DQD in a thin free-standing slab, which is an optical and phonon cavity (see notations in the text).

Let the energy difference Δ_1 between hybridised DQD levels be close to the frequencies ω_{LAq} of a set of $q = 1 - N$ acoustic phonon modes. We also assume a weak coupling between the acoustic phonons and DQD electron, which provides low mode population: $n_{LAq} \leqslant 1$. At the initial instant the microcavity contains one photon, which is necessary for implementing single-qubit rotations [8]. The dissipative effects, which are related to the photon escape from the cavity and anharmonic decay of slab phonon modes, are phenomenologically introduced into the Hamiltonian H_0 of the Schrödinger equation by adding an imaginary part to the corresponding frequencies:

$$H_0 = \sum_{i=0,1,-,+} \varepsilon_i |i\rangle\langle i| + (\omega_c - i\kappa) a^\dagger a + (\omega_{LO} - i\gamma_{LO}) b_{LO}^\dagger b_{LO} + \sum_{q=1}^{N} (\omega_{LAq} - i\gamma_{LAq}) b_{LAq}^\dagger b_{LAq}, \quad (1)$$

where ε_i ($i = 0,1,-,+$) are the energies of four DQD states; $a(a^\dagger)$ is the photon annihilation (creation) operator in the microcavity; $b_{LAq}(b_{LAq}^\dagger)$ is the phonon annihilation (creation) operator in the acoustic mode q; $b_{LOq}(b_{LOq}^\dagger)$ is the phonon annihilation (creation) operator in the optical mode; and κ, γ_{LAq}, and γ_{LO} are, respectively, the decay rates of the microcavity and phonon modes. Hereinafter, we assume that $\hbar = 1$. The energy exchange between the microcavity and DQD is described by the extended Jaynes–Cummings Hamiltonian:

$$H_{JC} = \Omega_{0-} a|-\rangle\langle 0| + \Omega_{0+} a|+\rangle\langle 0| + \Omega_{1-} a|-\rangle\langle 1| + \Omega_{1+} a|+\rangle\langle 1| + \text{H.c.}, \quad (2)$$

where Ω_{0-}, Ω_{0+}, Ω_{1-}, and Ω_{1+} are the interaction coefficients of the electron and microcavity photon (Rabi frequencies). The interaction Hamiltonian of the DQD and LO phonon has a similar form:

$$H_{e-LO} = g_{0-} b_{LO}|-\rangle\langle 0| + g_{0+} b_{LO}|+\rangle\langle 0| + g_{1-} b_{LO}|-\rangle\langle 1| + g_{1+} b_{LO}|+\rangle\langle 1| + \text{H.c.}, \quad (3)$$

where g_{0-}, g_{0+}, g_{1-}, and g_{1+} are the interaction coefficients of the electron and the slab optical mode. With regard to the contact between the electron and the acoustic modes, it may occur for only a transition between hybridised levels, whose splitting is on the order of 1–5 meV, and the corresponding interaction Hamiltonian can be written as

$$H_{e-LA} = \sum_{q=1}^{N} g_{LAq} b_{LAq} |+\rangle\langle -| + \text{H.c.}, \quad (4)$$

where g_{LAq} is the interaction coefficient between the electron and acoustic phonon of mode q.

The total Hamiltonian of the electron–photon–phonon system has the form

$$H = H_0 + H_{JC} + H_{e-LA} + H_{e-LO}. \quad (5)$$

The Schrödinger equation

$$i\frac{\partial}{\partial t}|\Psi\rangle = H|\Psi\rangle \quad (6)$$

with Hamiltonian (5) sets the evolution of the state vector $|\Psi\rangle$ of the system. This vector can be presented as an expansion

$$|\Psi\rangle = \sum_{k=1}^{M} c_k |k\rangle$$

over basis vectors

$$|k\rangle = |i\rangle \otimes |n_c\rangle \otimes |n_{LO}\rangle \otimes \prod_{q=1}^{N} |n_{LAq}\rangle,$$

where $k = 1 - M$; n_{LO} is the population of the LO phonon mode; and n_c is the population of the cavity mode. The dimension of the model Hilbert space with allowance for the conditions $n_{LAq} + n_{LO} \leqslant 1$ (no more than one vibrational quantum in the system) and $n_{LO} \leqslant 1$ (no more than one optical quan-

tum in the system) is $M = 6(N + 1) + 2$. It is convenient to pass to the frame of reference related to the microcavity using the unitary transformation

$$T = \exp[-i\omega_c(|-\rangle\langle -| + |+\rangle\langle +| + a^\dagger a + b_{LO}^\dagger b_{LO})t],$$

In this case, the Hamiltonian H_0 takes the form

$$\tilde{H}_0 = T^\dagger H_0 T + i\frac{\partial T^\dagger}{\partial t} T = \Delta_0 |1\rangle\langle 1| + \delta |-\rangle\langle -|$$

$$+ (\delta + \Delta_1)|+\rangle\langle +| - i\kappa a^\dagger a + (\Delta_{LO} + \delta - \Delta_0 - i\gamma_{LO}) b_{LO}^\dagger b_{LO}$$

$$+ \sum_{q=1}^{N} (\omega_{LAq} - i\gamma_{LAq}) b_{LAq}^\dagger b_{LAq}. \quad (7)$$

Here, $\Delta_0 = \varepsilon_1 - \varepsilon_0$ is the energy difference between the DQD ground states; $\Delta_1 = [V^2 + (\varepsilon_{A1} - \varepsilon_{B1})^2]^{1/2}$ is the energy difference between the DQD hybridised states; V is the tunnelling matrix element between the excited states $|A1\rangle$ and $|B1\rangle$ of isolated QDs (A and B in Fig. 1) with energies ε_{A1} and ε_{B1}, respectively; $\delta = \omega_0 - \omega_c$ is the microcavity frequency detuning from the transition frequency $|0\rangle \leftrightarrow |-\rangle$; and $\Delta_{LO} = \omega_{LO} - \omega_1$ is the LO mode frequency detuning from the transition frequency $|1\rangle \leftrightarrow |-\rangle$. Recall that the hybridised states $|-\rangle$ and $|+\rangle$ are related to the excited states $|A1\rangle$ and $|B1\rangle$ as

$$|-\rangle = \alpha|A1\rangle + \sqrt{1-\alpha^2}\,|B1\rangle, \quad |+\rangle = \sqrt{1-\alpha^2}\,|A1\rangle - \alpha|B1\rangle,$$

where $\alpha = \sin(\theta/2)$ and $\theta = \arctan(2V/\Delta_1)$.

Let us indicate the main DQD, microcavity, and phonon mode parameters corresponding to real low-dimensional QD-based systems. For crystalline vertical GaAs-based DQDs with a radius $R = 5-10$ nm and barrier thickness $L = 10-15$ nm, at a potential-well depth $U = 0.2-0.3$ eV, the transition frequency ω_{0-} between the ground and excited levels is 0.1 eV. The location of hybridised levels near the barrier edge causes their significant tunnel splitting with an energy $V \approx 1-5$ meV. The estimate $d_a \approx eR$ for the matrix elements of the operator optical dipole transition and the typical values of single-photon field amplitudes $E_c \approx 1-10$ V cm^{-1} yield an approximate value of 10^{-6} eV for the DQD Rabi frequencies Ω_{0-}, Ω_{0+}, Ω_{1-}, and Ω_{1+}. Concerning the interaction coefficients between the electron and phonon modes, their values are set by the type of the structure containing the DQD and the mutual frequency detunings for the DQD transitions, microcavity mode, and phonon modes. For example, if the DQD is located in a (100–1000)-nm-thick slab, one can suppress (or, vice versa, enhance) the interaction of the excited electron with LA phonons by choosing an appropriate geometry of the system [16]. The photon dissipation rate $\kappa \approx 10^{-5}-10^{-6}$ eV corresponds to the observed values for high-Q semiconductor microcavities.

In Sections 3 and 4 we present the calculation results specifying the influence of each of the aforementioned processes, which are related to the energy exchange between the DQD, microcavity, and phonons, on the DQD coherent dynamics. A DQD located at the centre of a thin slab is considered as a specific example of a real system; eigenfrequencies of the acoustic modes and interaction coefficients with the DQD electron were found for this DQD. The dynamics was simulated both for this structure and for a system with averaged characteristics. All parameters in these sections are given in units of microcavity frequency ω_c, which was assumed to be fixed and equal to 0.1 eV.

3. Interaction between DQD and localised acoustic phonons in a thin slab

Since quantum coherence is a necessary requirement for a physical system considered as a qubit, one should not only develop ways for implementing quantum operations but also study the parasitic effect of external noise. One of the main sources of coherence loss in QD-based charge qubits is the electron–phonon interaction, which leads to relaxation and dephasing of electronic states in the QD [1, 2]. One of the ways to control the electron–phonon interaction is to convert the frequency spectrum of mechanical vibrations. The phonon spectrum of confined structures (nanocrystals, thin slabs) differs from that of bulk materials, in particular, by the formation of subbands (branches). Modern technologies make it possible to design structures of different profiles and sizes, for example, thin free-standing membranes, interacting with the rest (massive) part of the sample only at fixing points. We will analyse the influence of phonons on the GaAs/InAs DQD placed in a thin slab at frequencies $\omega_0 \leqslant 1$ meV, corresponding to the transition frequency Δ_1 of the electron between split excited levels. To this end, the mechanical vibration spectrum and the contribution of each phonon branch to the electron–phonon interaction for slabs of different thicknesses will be calculated.

According to [16, 18–20], we will apply the model describing the interaction between Lamb waves and a DQD located in the middle of a thin slab. The latter is almost completely separated from the rest of the material (substrate), so that acoustic vibrations are entirely limited by the upper and lower faces. If we neglect the perturbations introduced by contact points between the slab and substrate, the slab behaves as a phonon cavity [21, 22]. Since we consider only the deformation interaction, two forms of Lamb modes (waves) arise: dilatation modes (compression) and bending modes. If the DQD is located in the central part of the slab, one can take into account only dilatation waves, because bending waves do not interact with the QD. The corresponding dispersion relations for the dilatation waves can be derived from the Rayleigh–Lamb equation (see, e.g., [21]):

$$\begin{cases} \dfrac{\tan t}{\tan l} = -\dfrac{4x^2 lt}{(x^2 - t^2)^2}, \\ c_{long}^2(x^2 + l^2) = c_{trans}^2(x^2 + t^2), \end{cases} \quad (8)$$

where c_{long} and c_{trans} are, respectively, the longitudinal and transverse velocities of acoustic waves in a three-dimensional semiconductor; $x = q_\parallel W/2$; $t = q_{trans} W/2$; $l = q_{long} W/2$; $q_\parallel$, q_{long}, and q_{trans} are, respectively, the lateral, longitudinal, and transverse components of the phonon wave vector (in the slab plane); and W is the slab thickness. System (8) has a set of solutions (branches) for t and l at each x value. The frequency of a branch with number n is determined by the expression

$$\omega_n = \frac{2c_{long}\sqrt{x^2 + l_n^2}}{W} = \frac{2c_{trans}\sqrt{x^2 + t_n^2}}{W}. \quad (9)$$

The phonon–DQD interaction coefficient has the form [16]

$$g_n = \lambda_n \mathcal{P}(\boldsymbol{q}_\parallel)[1 - \exp(-i\boldsymbol{q}_\parallel \boldsymbol{d})], \quad (10)$$

where $\boldsymbol{d}$ is the vector connecting the centres of two QDs. The form factor for a QD with a radius R is given by the formula

$$\mathcal{P}(\boldsymbol{q}_{\|}) = \int n_e(\boldsymbol{r}) \exp(-i\boldsymbol{q}_{\|}\boldsymbol{r}_{\|}) d^3r = \exp\left(-\frac{2x^2R^2}{W^2}\right), \qquad (11)$$

and the electron charge density distribution is assumed to be Gaussian:

$$n_e(\boldsymbol{r}) = \delta(z)\frac{1}{2\pi R^2}\exp\left(-\frac{r_{\|}^2}{2R^2}\right), \qquad (12)$$

where $n_e(\boldsymbol{r})$ is the Dirac $\delta(z)$ function. Thus, the interaction coefficient can be written as

$$g_n = \lambda_n \exp\left(-\frac{2x^2R^2}{W^2}\right)\left[1 - \exp\left(-i\frac{4xd\cos\theta}{W}\right)\right]. \qquad (13)$$

The quantity

$$\lambda_n = F_n \frac{16}{W^4}\sqrt{\frac{\hbar E_\alpha^2}{2A_s\rho\omega_n}}(t_n^2 - x^2)(l_n^2 + x^2)\sin t_n$$

describes the interaction intensity between an electron and dilatation LA phonons. Here, E_α is the deformation potential constant, A_s is the slab area, and ρ is the semiconductor density; the normalisation constant F_n is calculated from the expressions reported in [22]. We used the following parameters for a GaAs QD: $E_\alpha = 2.2 \times 10^{-18}$ J, $\rho = 5.3 \times 10^3$ kg m^{-3}, $c_{trans} = 3.35 \times 10^3$ m s^{-1}, $c_{long} = 5.7 \times 10^3$ m s^{-1}, $A_s = 1$ μm^2, $R =$ 10 nm, and $d = 30$ nm.

The dependences of frequencies ω_n of eigenmodes on the parameter $x = q_{||}W/2$ for a slab of thickness $W = 400$ nm are shown in Fig. 2. According to expression (9), the number of branches in the range $\omega \leqslant 1$ meV is proportional to the thickness W; it is equal to 46 at $W = 400$ nm. The branches make different contributions to the electron–phonon interaction. System (8) was analysed in detail in [21]; it was shown that, depending on x, there are several types of solutions: (i) l_n and t_n are purely imaginary, (ii) l_n is imaginary and t_n is real, and (iii) l_n and t_n are real. A calculation of the electron–phonon interaction coefficient (13) shows that, in the case of imaginary l_n and t_n, the g_n magnitude is many orders of magnitude smaller than for real l_n and t_n. This disproportion is related to a decrease in the normalisation constant F_n because of a sharp increase in the exponential term [22]. Similar results were obtained for slabs with thicknesses $W = 200$ and 600 nm. Thus, all branches of the phonon spectrum must be taken into account at small x, whereas at large x only upper branches contribute to the resulting interaction.

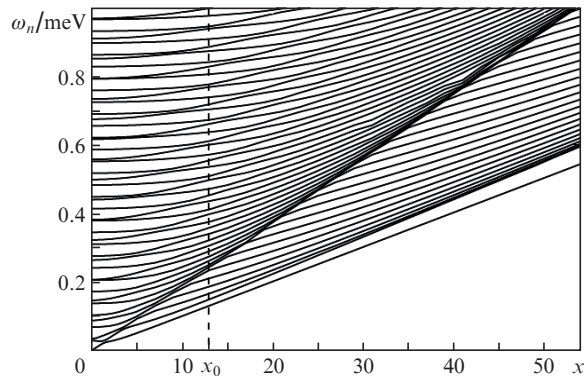

Figure 2. Spectrum of phonon eigenmodes for a GaAs slab.

4. Influence of electron–phonon exchange in an excited DQD on the implementation of a quantum gate 'NOT'

Based on the results obtained in Section 3, we will analyse the electron dynamics in a DQD and microcavity with allowance for the exchange of a quantum between the symmetric ($\Delta_0 = \Delta_1 = 0$) DQD and a set of acoustic phonon modes. Let us consider the $|0\rangle \otimes |1\rangle_c \otimes |0_{LO}\rangle \otimes |0_{LA\,1}\rangle \ldots |0_{LA\,N}\rangle$ state as the initial one and tune the transition frequency from the $|0(1)\rangle$ level to the $|+\rangle$ level in the DQD in resonance with the microcavity frequency. Note that tuning the transition frequency from the $|0(1)\rangle$ level to the $|-\rangle$ level in resonance with the microcavity frequency does not lead to an energy exchange with phonon modes. The reason is that all reservoir modes are not populated initially, and the DQD cannot absorb an energy quantum that is necessary to induce the $|-\rangle \to |+\rangle$ transition. Thus, at a sufficiently high degree of phonon spectrum discretisation and a low temperature, one can isolate the DQD from the influence of acoustic modes by choosing the $|-\rangle$ state as a transport one. The frequency of the optical phonon mode is detuned from the transition frequency in the DQD and barely affects the evolution of the state vector of the system.

Let us solve numerically Eqn (6) for different slab thicknesses W (Fig. 2). For example, Fig. 3 shows (hereinafter, it is assumed that $\Omega_{0(1)+} = \Omega_{A(B)}$) the time dependences of the populations P_i of DQD states for some set of parameters at a thickness satisfying the condition $x = x_0$. In this case, the symmetric DQD is controlled by only the single-photon microcavity field. It can be seen that the electron transfer between the logical states through the transport level $|+\rangle$ is accompanied by undesirable population of the lower hybridised level $|-\rangle$ due to the resonance excitation of the phonon subsystem that is in the vacuum state. In fact, this process involves several LA modes, whose frequencies are in the close proximity of the transition frequency between hybridised levels. To demonstrate the influence of the entire phonon reservoir on the electron transfer, we will plot the dependence of the maximum population of the final state $|1\rangle$ on the tunnelling energy

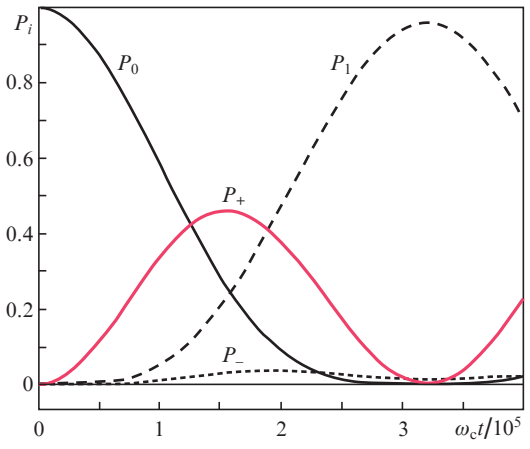

Figure 3. Time dependences of the populations P_i of four states of a symmetric DQD for a set of phonon reservoir frequencies corresponding to the dashed line $x = x_0$ in Fig. 2. The parameters of the system are as follows: $V = 0.25 \times 10^{-2}$, $\Delta_0 = 0$, $\Delta_{LO} = 10^{-3}$, $\Omega_{A(B)} = 10^{-5}$, and $\kappa = \gamma_{LA} = \gamma_{LO} = 10^{-7}$.

V, which determines the splitting of hybridised levels for choosing the slab thickness satisfying the condition $x = x_0$. If the energies of the $|A1\rangle$ and $|B1\rangle$ states coincide exactly, the transition frequency between them is $2V$. Varying it in the frequency range of slab acoustic modes, one can see how each of them affects the electron dynamics. When scanning energy V, the dependence of $\max P_1$ on Δ_1 demonstrates a sequence of minima (Fig. 4), which correspond to the frequencies of LA modes; their magnitudes are determined by the interaction coefficients g_n: the larger these coefficients, the smaller the $\max P_1$ values.

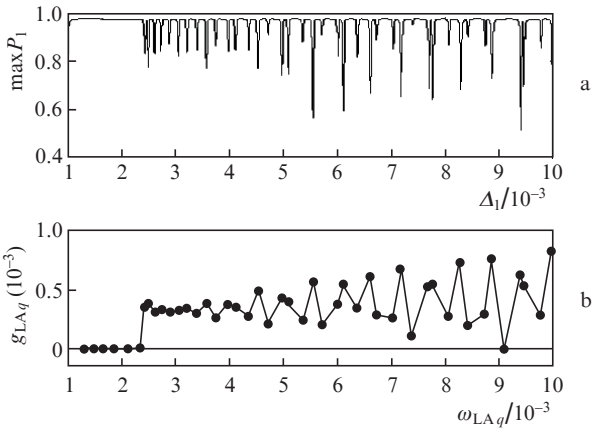

Figure 4. Dependences of (a) the maximum transfer probability on the transition frequency between split levels in the DQD and (b) the interaction energy of an electron with slab acoustic modes on the frequency ω_{LAq} ($N = 46$). The parameters of the system are as follows: $\Delta_0 = 0$, $\Delta_{LO} = 10^{-3}$, $\Omega_{A(B)} = 10^{-5}$, and $\kappa = \gamma_{LO} = \gamma_{LAq} = 10^{-7}$.

For thicker slabs, the phonon frequencies come closer together to form a quasi-continuum, which exhibits properties of a Markovian reservoir. In this case, the spectrum of the phonon subsystem is simulated as follows. We are primarily interested in the frequency range with a centre frequency Δ_1, corresponding to the energy difference between the hybridised levels $|-\rangle$ and $|+\rangle$. Choosing the frequency range X at a fixed number of modes N, one links the density of phonon modes with the spacing between neighbouring modes, $\Delta_m = X/(N-1)$; the mode frequencies in the equidistant spectrum of LA phonons are $\omega_{LAq} = \Delta_1 - X/2 + (q-1)\Delta_m (q = 1-N)$. The phonon mode decay rate γ_{LAq} is set by using experimental data and is varied in the range of $\sim 10^{-6}$–10^{-9} eV. In this study, we assume for simplicity the quantum exchange rates between the DQD and phonons and the decay rates to be identical for all modes (white noise approximation): $g_{LAq} \equiv g_{LA}$ and $\gamma_{LAq} \equiv \gamma_{LA}$.

Under low-temperature conditions, the probability of absorbing a thermal phonon by a QD is much lower than the probability of emitting a phonon by an excited electron. Therefore, if the lower hybridised state is chosen as a transport one, the electron transfer will be subjected to relaxation to a smaller extent. The interaction energy (quantum exchange rate) between the DQD and a set of phonon modes is proportional to the population of modes and their density at the transition frequency. In turn, the population is determined by the ratio of the mode frequency to temperature and by the population mechanism. For example, for a thermal (Poisson) field, the probability of finding n_{ph} phonons in a mode is $P_{therm}(n_{ph}) = \bar{n}^{n_{ph}}/(1+\bar{n})^{n_{ph}+1}$, while the probability for a coherent field (formed, e.g., by a resonance microwave monochromatic source) is $P_{coh}(n_{ph}) = \bar{n}^{n_{ph}} \exp(-\bar{n})/n_{ph}!$ (here, $\bar{n} = [\exp(\omega_q/\Theta) - 1]^{-1}$ is the average number of phonons with a frequency ω_q at a temperature Θ). We are interested in the the case where the average number of phonons in a mode does not exceed 1 (Fig. 5).

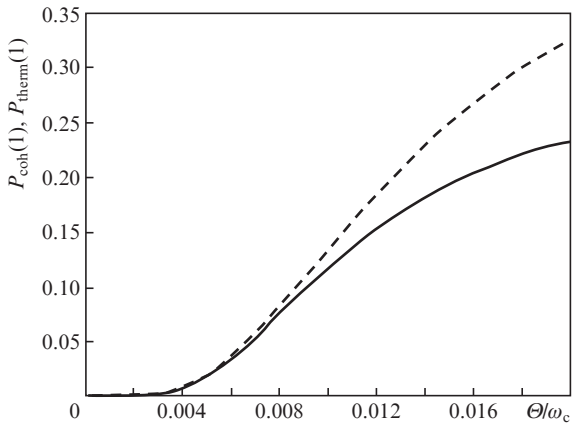

Figure 5. Dependences of the populations $P_{coh}(1)$ (dashed line) and $P_{therm}(1)$ (solid line) of one-phonon states on temperature Θ for coherent and thermal fields.

Let us consider the influence of acoustic phonons on the electron transfer in our coherent model. Now, the optical transitions in an asymmetric DQD are independently controlled by the single-photon field of microcavity and the one-phonon field of the LO mode (see Fig. 1), and the reversible energy exchange with LA phonons occurs at a transition between hybridised levels. The initial state of a phonon mode with a frequency ω_q can be written as $|\Psi\rangle_{LAq} \approx \sqrt{1-P(1)}\,|0\rangle_q + \sqrt{P(1)}\,|1\rangle_q$; here, the possibility of populating states with $n_q > 1$ is neglected. In total, $N = 10$ modes in the vicinity of the transition frequency Δ_1 with a width $g_{LA} = 10^{-6}$ were taken into account. The calculation results (Fig. 6) indicate a monotonic decrease in the transfer probability, beginning with the Θ values approximately corresponding to liquid helium temperature. For a coherent phonon field, this decrease is larger than that for a thermal field. At low temperatures, the main factor determining the $\max P_1$ value is the choice of the transport level. As one would expect, the transfer probability is higher for the lower hybridised state (the losses are determined entirely by the photon drift from the microcavity). With an increase in temperature, the peak magnitude begins to depend on the initial state of the phonon subsystem; for a coherent field, it decreases more rapidly than for a thermal one.

Let us now analyse the dependence of the transfer probability on the decay rate γ_{LA} of acoustic modes for two g_{LA} values. It is reasonable to assume that this probability decreases with increasing decay rate. However, one can see that at very high rates ($\gamma_{LA} > 10^{-4}$) the transfer probability increases and tends to values characteristic of the DQDs in which the coupling with LA phonons is suppressed (Fig. 7, dashed line). In this case, the phonon mode density is rather high (20 modes per $0.01V$). This result can be explained as follows. According to the Jaynes–Cummings model, where the dissipation is phenomenologically taken into account within the Schrödinger equation formalism, the decay rates of

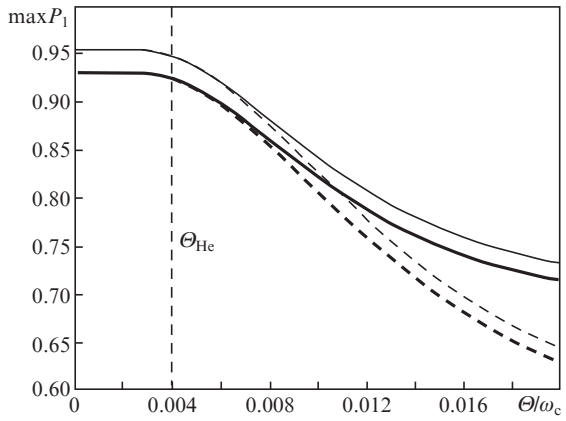

Figure 6. Dependences of maxP_1 on temperature Θ for coherent (dashed lines) and thermal (solid lines) initial states of phonon field and for two transport states: lower state $|0\rangle \leftrightarrow |-\rangle \leftrightarrow |1\rangle$ (thin lines) and upper state $|0\rangle \leftrightarrow |+\rangle \leftrightarrow |1\rangle$ (bold lines). The vertical dashed line corresponds approximately to liquid helium temperature $\Theta_{He} = 4.2$ K. The parameters of the system are as follows: $V = 10^{-2}$, $\Delta_0 = -10^{-1}$, $\Omega_{A(B)} = g_{LO} = 10^{-5}$, $\kappa = \gamma_{LA} = \gamma_{LO} = 10^{-7}$, and $N = 10$.

the photon and electron subsystems play the role of effective detunings. The parameters chosen for Fig. 7 correspond to a symmetric DQD controlled by the single-photon field of microcavity, and the phonon modes are considered as a reservoir. An increase in the decay rate of LA modes by several orders of magnitude detunes them from resonance with the DQD, thus blocking this dissipative channel.

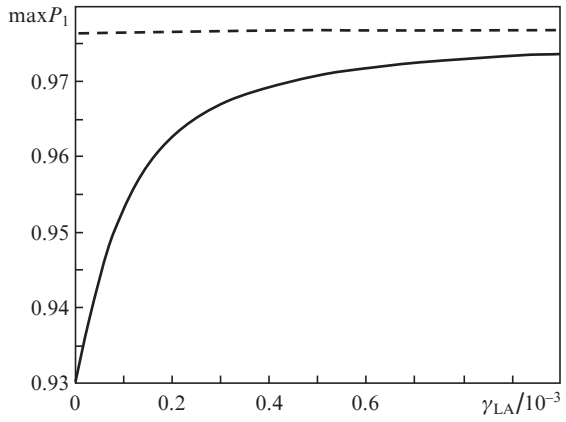

Figure 7. Dependences of maxP_1 on the decay rate of LA phonons for strong (solid line) and weak (dashed line) interaction between modes and DQD. The parameters of the system are as follows: $V = 10^{-2}$, $\Delta_0 = 0$, $\Delta_{LO} = 10^{-3}$, $\Omega_{A(B)} = g_{LO} = 10^{-5}$, $\kappa = \gamma_{LO} = 10^{-7}$, and $N = 20$.

5. Conclusions

Traditionally, acoustic and optical phonons in solid-state systems form the main channel of coherence loss, and serve an essential source of errors in quantum calculations based on charge qubits. This is primarily due to the continuum type of the phonon frequency spectrum, which is described within the Markovian approach. However, since the phonon mode spectrum for devices with characteristic sizes less than 1 μm is quasi-discrete, we can speak about coherent interaction (reversible exchange of energy) between the electron system (qubit) and phonon modes. On the one hand, this circumstance allows one to use these modes as an auxiliary tool for controlling the qubit state. At the same time, an increase in the spectrum discretisation and enhancement of localisation of mechanical (deformation) energy lead to enhanced interaction of the DQD electron with a large number of modes, as a result of which the qubit evolution may deviate from the calculated one. A descriptive example of this phonon system is a set of Lamb eigenmodes of a slab-like membrane.

A theoretical analysis of the dynamics of a single-electron DQD in an optical microcavity was performed taking into account the influence of optical and acoustic phonons. Lamb modes in a thin GaAs slab were considered as an example of an acoustic phonon subsystem, and the phonon spectrum frequencies and phonon–electron interaction coefficients were determined. The processes related to the phonon influence were found to modify to a certain extent the quantum evolution of this system. Generally, such a modification manifests itself as a decrease in the transfer probability with an increase in the interaction energies because of the 'mixing' of excited DQD levels when their splitting energy coincides with the frequency of one of acoustic modes. Calculations were performed for a specific set of individual slab modes (up to 50 in number) and in the white noise approximation, where all modes are assumed to be identical. One can note the dependence of the electron transfer probability between the QDs (the 'NOT' probability) on the initial state of the acoustic subsystem. In addition, an increase in the mode decay rate blocks the coupling between the DQD and phonons. A scenario of charge qubit control with combined photon–phonon control was also considered. As follows from the calculations, the optical phonon mode of slab can efficiently be used to exert a resonance effect on a qubit and design a 'NOT' gate. Further on, a more detailed consideration of the specific features of the phonon spectrum (for example, in a rod or in a slab) will make it possible to calculate more accurately the dissipation rate and gain a better insight into the processes occurring in an optically controlled DQD.

Acknowledgements. We are grateful to M.S. Rogachev for his help in numerical calculations.

The study was carried out under the programme of the Ministry of Science and Higher Education of the Russian Federation.

References

1. Fedichkin L., Yanchenko M., Valiev K.A. *Nanotechnology*, **11**, 387 (2000).
2. Hu X., Koiller B., Das Sarma S. *Phys. Rev. B*, **71**, 235332 (2005).
3. Burkard G., Loss D., DiVincenzo D.P. *Phys. Rev. B*, **59**, 2070 (1999).
4. Tsukanov A.V., Valiev R.A. *Mikroelektron.*, **36**, 83 (2006).
5. Hayashi T., Fujisawa T., Cheong H.D., Jeong Y.H., Hirayama Y. *Phys. Rev. Lett.*, **91**, 226804 (2003).
6. Lu X.-Y., Wu J., Zheng L.-L., Zhan Z.-M. *Phys. Rev. A*, **83**, 042302 (2011).
7. Tsukanov A.V., Openov L.A. *Fiz. Tekh. Poluprovodn.*, **38**, 94 (2004).
8. Tsukanov A.V., Kateev I.Yu. *Mikroelektron.*, **42**, 246 (2013).
9. Jacak L., Machnikowski P., Krasnyj J., Zoller P. *Eur. Phys. J. D*, **22**, 319 (2003).
10. Urayama J., Norris T.B. *Phys. Rev. Lett.*, **86**, 4930 (2001).

11. Grange T., Ferreira R., Bastard G. *Phys. Rev. B*, **76**, 241304 (2007).
12. Zibik E.A., Grange T., Carpenter B.A., Porter N.E., Ferreira R., Bastard G., Stehr D., Winner S., Helm M., Liu H.Y., Skolnick M.S., Wilson L.R. *Nat. Mater*., **8**, 803 (2009).
13. Krauss T.D., Wise F.W. *Phys. Rev. Lett*., **79**, 5102 (1998).
14. Ortner G., Oulton R., Kurtze H., Schwab M., Yakovlev D.R., Bayer M., Fafard S., Wasilewski Z., Hawrylak P. *Phys. Rev. B*, **72**, 165353 (2005).
15. Li X.-Q., Nakayama H., Arakawa Y. *Phys. Rev. B*, **59**, 5069 (1999).
16. Liao Y.Y., Chen Y.N., Chou W.C., Chuu D.S. *Phys. Rev. B*, **77**, 033303 (2008).
17. O'Connell A.D., Hofheinz M., Ansmann M., Bialczak R.C., Lenander M., Lucero E., Neeley M., Sank D., Wang H., Weides M., Wenner J., Martinis J.M., Cleland A.N. *Nature*, **464**, 697 (2010).
18. Jua W.-M., Zhu K.-D., Huang P.-H., Zheng H. *Eur. Phys. J. B*, **72**, 417 (2009).
19. Debald S., Brandes T., Kramer B. *Phys. Rev. B*, **66**, 041301 (2002).
20. Liao Y.Y., Chen Y.N. *Phys. Rev. B*, **81**, 153301 (2010).
21. Bannov N., Aristov V., Mitin V. *Phys. Rev. B*, **51**, 9930 (1995).
22. Bannov N., Mitin V., Stroscio M. *Phys. Status Solidi B*, **183**, 131 (1994).